Geophysical Prospecting, 2005, **53**, 803–810

Estimation of gas-hydrate concentration and free-gas saturation at the Norwegian-Svalbard continental margin

José M. Carcione,* Davide Gei, Giuliana Rossi and Gianni Madrussani

Istituto Nazionale di Oceanografia e di Geofisica Sperimentale (OGS), Borgo Grotta Gigante 42c, 34010 Sgonico, Trieste, Italy

Received August 2004, revision accepted November 2004

ABSTRACT

We estimate the concentration of gas hydrate and free gas at an area located to the north of the Knipovich Ridge (western Svalbard margin). The method is based on P-wave velocities computed by reflection tomography applied to multicomponent ocean-bottom seismometer data. The tomographic velocity field is fitted to theoretical velocities obtained from a poro-elastic model based on a Biot-type approach (the interaction between the rock frame, gas hydrate and fluid is modelled from first physical principles). We obtain average hydrate concentrations of 7% and maximum free-gas saturations of 0.4% and 9%, depending on the saturation model.

INTRODUCTION

Gas hydrate is composed of water and natural gas, mainly methane, which forms under conditions of low temperature, high pressure and proper gas concentration (Kvenvolden 1993). Bottom-simulating reflectors on seismic profiles are interpreted as representing the seismic signature of the base of gas-hydrate formation: a free-gas zone may be present just below the bottom-simulating reflector (Stoll, Ewing and Bryan 1971; Lodolo, Camerlenghi and Brancolini 1993). The worldwide mapping of gas hydrate is important, because it is a potential energy resource, and can be the cause of slope failure offshore (a submarine geohazard) (Mienert and Posewang 1999) and an important issue in global warming (the greenhouse effect) (Grevemeyer and Villinger 2001).

The Knipovich Ridge, located between the Greenland and Svalbard margins, represents the extension of the mid-Atlantic Ridge (Lundin and Doré 2002) (Fig. 1). In this area, with a total organic content of nearly 1% (Butt *et al.* 2000), gas generation and flow are responsible for the presence of methane gas hydrate and bottom-simulating reflectors at a depth of nearly 100–200 m below the sea-bottom (Posewang and Mienert 1999; Vanneste *et al.* 2002). Moreover, the combination of overpressured gas and neo-tectonic activity is the probable cause of mud diapirism mainly observed in the southwest of the Svalbard margin (Brown 1990).

The area to the north of the Knipovich Ridge was surveyed by the RV *Jan Mayen* from the University of Tromsø during the summer of 2001. The study area lies between the Molloy Transform and the Vestnesa Ridge on the northern part of the Knipovich Ridge (see Fig. 1). Data acquisition consisted of single-channel high-resolution seismic and ocean-bottom seismometer (OBS) data. The distance between seismic lines was 200 m and 20 OBSs were positioned every 400 m (offsets up to 5 km were obtained). The source consisted of two sleeve guns (0.65 l per gun) towed at 4 m depth below the surface. The frequency range of the source was [30,450] Hz, with spectral notches at 180 and 360 Hz. The reflections beneath the bottom-simulating reflector are characterized by a polarity reversal, high amplitudes and low-frequency content, which can be attributed to the accumulation of free gas below the hydrate zone. These features can be observed in Fig. 2, which shows down-slope (a) and along-slope (b) seismic profiles. These profiles are indicated by thick lines in Fig. 1. The bottom-simulating reflector, although discontinuous, can be clearly seen in the down-slope profile between 2.0 and 2.4 s (nearly 200 m below the sea-bottom), and cuts obliquely across the bedding reflectors.

We processed the OBS data using traveltime reflection tomography and we obtained a P-wave velocity cube (Rossi, Madrussani and Camerlenghi 2003). The discrepancies

*E-mail: jcarcione@ogs.trieste.it

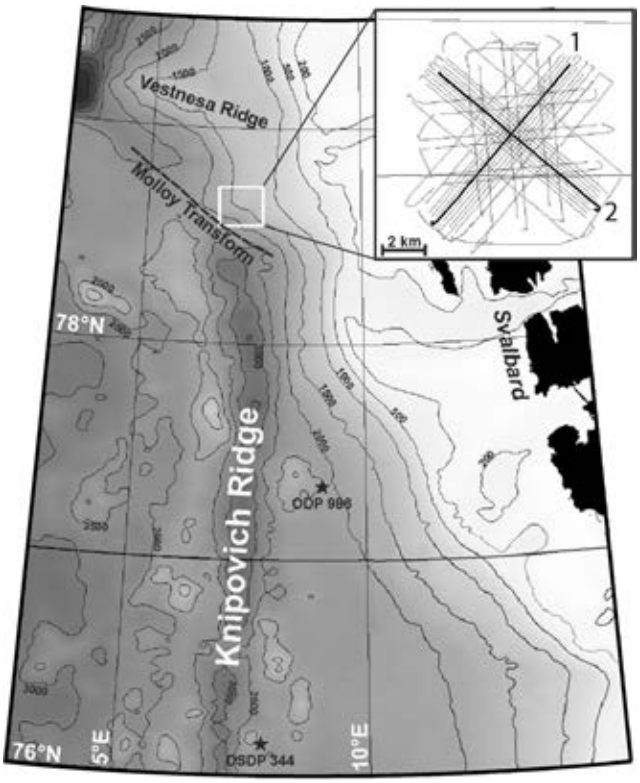

Figure 1 Bathymetric map of the western Svalbard margin and study area (Vanneste *et al.* 2002). The thick perpendicular lines correspond to the seismic profiles used in this work.

between the tomographic velocity profile and the velocity for water-filled, normally compacted, marine sediments are interpreted as being due to the presence of gas hydrate (positive anomalies) and free gas (negative anomalies). These anomalies can be translated in terms of concentration of clathrate and free gas, knowing the velocity trend versus gas-hydrate and free-gas content (Gei and Carcione 2003; Carcione and Gei 2004; Chand *et al.* 2004).

ROCK-PHYSICS MODEL

Wave velocity is an important property which can give information about lithology, saturation, and the *in situ* conditions of rocks. Carcione and Tinivella (2000) modelled the acoustic properties of gas-hydrate-bearing sediments saturated with water in the framework of Biot's theory of poro-elasticity. The original theory, for frozen porous media, was proposed by Leclaire, Cohen-Ténoudji and Aguirre-Puente (1994), and confirmed by Leclaire, Cohen-Ténoudji and Aguirre-Puente (1995) with laboratory experiments. Unlike previous theories, based simply on slowness and/or moduli averaging of two-phase models, the Biot-type three-phase theory considers the existence of two solids (grains and gas hydrate) and a fluid. The resulting P-wave dispersion relationship constitutes a generalization of the Gassmann equation for two frames and one fluid. The model is based on the assumption that hydrate fills the pore space and shows interconnections.

We consider the low-frequency limit of the theory, thus neglecting dissipation. At this limit, grains, hydrate and water move in phase. In this case, the equations have a simplified form. We denote the grains, hydrate and water by the subscripts s, h and w, and we let ϕ, K, μ and ρ denote material proportion (or fraction), bulk modulus, shear modulus and density, respectively. The gas-hydrate concentration is defined as

$$S_{\rm h} = \frac{\phi_{\rm h}}{\phi}, \tag{1}$$

where $\phi = \phi_{\rm h} + \phi_{\rm w}$ is the actual rock porosity. Hence, the fraction of each component can be expressed as

$$\begin{aligned} \phi_{\rm h} &= \phi S_{\rm h}, \\ \phi_{\rm w} &= \phi(1 - S_{\rm h}), \\ \phi_{\rm s} &= 1 - \phi. \end{aligned} \tag{2}$$

If $K_{\rm sm}$ and $K_{\rm hm}$ denote the bulk moduli of the rock and hydrate frames, the bulk modulus of the closed system can be expressed as

$$K_{\rm G} = K_{\rm sm} + K_{\rm hm} + \left(1 - \frac{K_{\rm sm}}{K_{\rm s}} - \frac{K_{\rm hm}}{K_{\rm h}}\right)^2 M, \tag{3}$$

where

$$M = \left[\left(\phi_{\rm s} - \frac{K_{\rm sm}}{K_{\rm s}}\right)\frac{1}{K_{\rm s}} + \frac{\phi_{\rm w}}{K_{\rm w}} + \left(\phi_{\rm h} - \frac{K_{\rm hm}}{K_{\rm h}}\right)\frac{1}{K_{\rm h}}\right]^{-1}. \tag{4}$$

The modulus $K_{\rm G}$ is a generalization of the Gassmann (low-frequency) modulus of the classical Biot theory (e.g. Carcione 2001, p. 225). The shear modulus of the composite is simply the sum of the moduli of the rock and hydrate frames (these are given below in equations (14) and (17), respectively),

$$\mu_{\rm m} = \mu_{\rm sm} + \mu_{\rm hm}. \tag{5}$$

The P- and S-wave velocities are then

$$v_{\rm P} = \sqrt{\frac{K_{\rm G} + 4\mu_{\rm m}/3}{\rho}} \quad \text{and} \quad v_{\rm S} = \sqrt{\frac{\mu_{\rm m}}{\rho}}, \tag{6}$$

where

$$\rho = \phi_{\rm s}\rho_{\rm s} + \phi_{\rm w}\rho_{\rm w} + \phi_{\rm h}\rho_{\rm h} \tag{7}$$

is the bulk density.

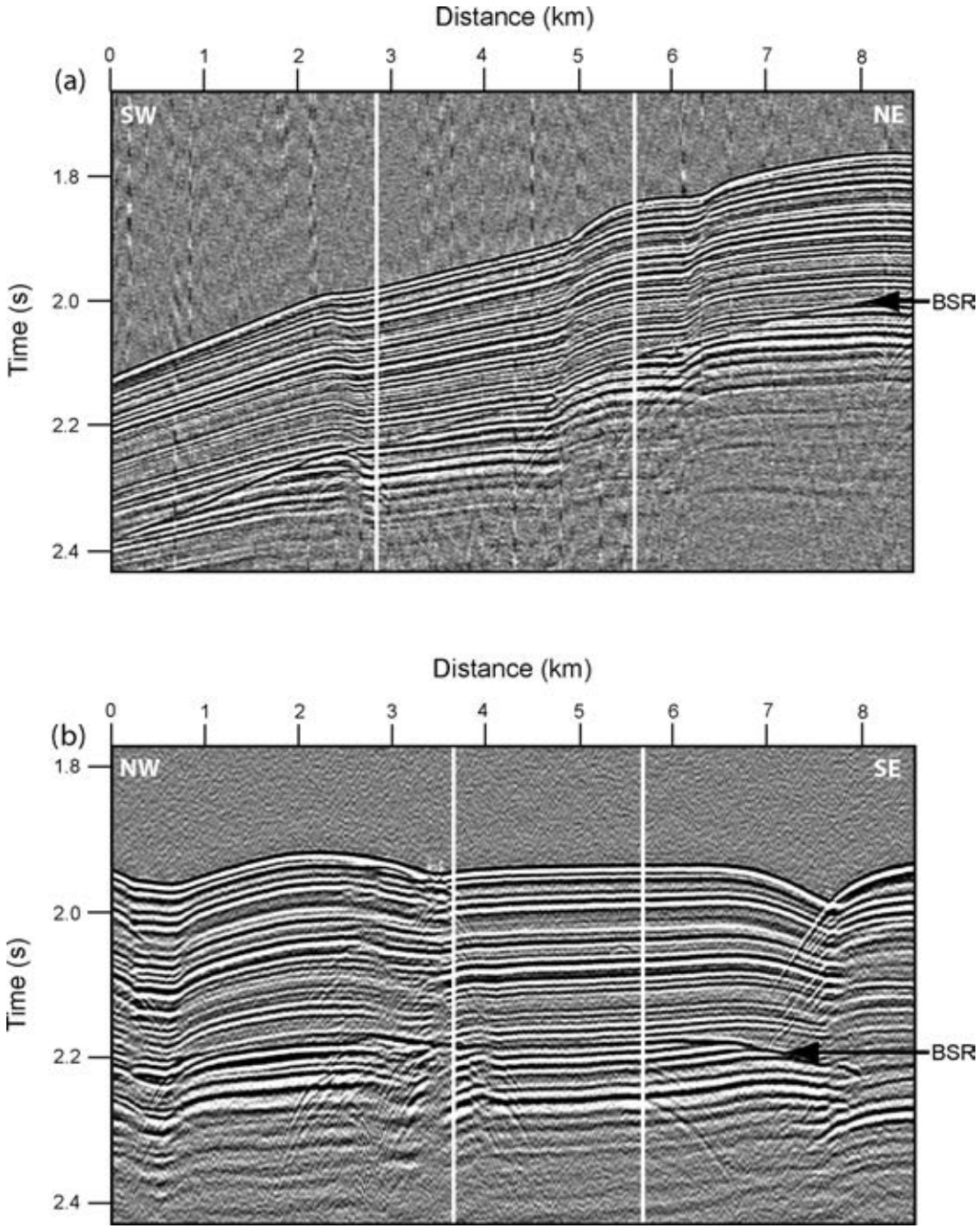

Figure 2 (a) Seismic profile 1 and (b) seismic profile 2 indicated in Fig. 1. The bottom-simulating reflector can be identified. The data have a lower frequency content below this reflection.

The presence of clay and calcite modifies the effective bulk modulus of the grains. That is, the grains are formed by a mixture of quartz, clay and calcite. If K_q, K_c and K_{ca} are the sand-grain, clay-particle and calcite bulk moduli, we assume that K_s is equal to the average of the upper and lower Hashin–Shtrikman bounds (Hashin and Shtrikman 1963). Defining the sand, clay and calcite fractions as ϕ_q, ϕ_c and ϕ_{ca}, respectively, the clay content as C and the calcite content as c, the following relationships hold:

$$\phi + \phi_q + \phi_c + \phi_{ca} = 1, \tag{8}$$

$$C = \frac{\phi_c}{\phi_c + \phi_q + \phi_{ca}} \tag{9}$$

and

$$c = \frac{\phi_{ca}}{\phi_c + \phi_q + \phi_{ca}}. \tag{10}$$

The Hashin–Shtrikman upper and lower bounds for the bulk and shear moduli, denoted by superscripts (+) and (−), respectively, are

$$K^{HS\pm} = \Lambda(\mu_\pm),$$
$$\mu^{HS\pm} = \Gamma[\xi(K_\pm, \mu_\pm)], \tag{11}$$

where

$$\Lambda(\mu_\pm) = \left\langle \frac{1}{K + \frac{4}{3}\mu_\pm} \right\rangle^{-1} - \frac{4}{3}\mu_\pm,$$
$$\Gamma(\xi) = \left\langle \frac{1}{\mu + \xi} \right\rangle^{-1} - \xi,$$
$$\xi(K_\pm, \mu_\pm) = \frac{\mu_\pm}{6}\left(\frac{9K_\pm + 8\mu_\pm}{K_\pm + 2\mu_\pm}\right)$$

(e.g. Mavko, Mukerji and Dvorkin 1998), and the subscripts (+) and (−) denote the maximum and minimum moduli of the three single constituents. The brackets $\langle \bullet \rangle$ indicate an average over the constituents weighted by their volume fractions. The average grain density is given by $\rho_s = (1 - C - c)\,\rho_q + C\rho_c + c\rho_{ca}$.

The dry-rock moduli K_{sm} and μ_{sm0} are estimated from the sonic-log profile at full water saturation. We use the inverse Gassmann equation to obtain the bulk modulus at two calibration points, K_{sm1} and K_{sm2}, obtained as

$$K_{sm} = \frac{(\phi K_s/K_w + 1 - \phi)K - K_s}{\phi K_s/K_w + K/K_s - 1 - \phi} \tag{12}$$

(Carcione 2001, p. 225), where $K = \rho V_P^2 - (4/3)\,\mu_{sm0}$ is the wet-rock modulus and V_P is the P-wave velocity. The shear modulus for $S_h = 0$ is equal to

$$\mu_{sm0} = \frac{3(1 - 2\nu)K}{2 + 2\nu}, \tag{13}$$

where ν is Poisson's ratio. The dry-rock modulus is assumed to vary with depth as $K_{sm} = K_0 + (K_\infty - K_0)[1 - \exp(-p_d/p^\star)]$, where $p_d = (\rho_s - \rho_w)(1 - \phi)\,zg$ is the differential pressure, z is the depth below the sea-floor and g is the acceleration of the earth's gravitational field. The values of K_0, K_∞ and $p^\star$, which are obtained by using the sonic log as calibration data, are functions of K_{sm1} and K_{sm2}.

We assume that the rigidity modulus of the rock frame is affected by cementation of the grains by gas hydrate. It is based on a percolation model where, in the absence of hydrate, the shear modulus is that at full water saturation (μ_{sm0}), and at 100% hydrate saturation the modulus is Kuster and Toksöz's (1974) shear modulus (μ_{mKT}), where the inclusion is air (isolated pores). Arbabi and Sahimi (1988) performed numerical simulations of elastic properties of 3D percolation networks. Using Monte-Carlo simulations and finite-size scaling analysis, they found that the percolation coefficient (see below) should be 3.78 with an error of about 3%. This critical value characterizes the power-law behaviour of the elastic moduli near the percolation threshold. We then consider

$$\mu_{sm} = \mu_{sm0} + (\mu_{mKT} - \mu_{sm0})(\phi_h/\phi)^p, \tag{14}$$

where p = 3.8 is the percolation coefficient,

$$\frac{\mu_{mKT}}{\mu_s} = \frac{(1 - \phi)(9K_s + 8\mu_s)}{9K_s + 8\mu_s + \phi(6K_s + 12\mu_s)} \tag{15}$$

(Kuster and Toksöz 1974), and the shear modulus of air is assumed to be zero.

Similarly, the moduli of the hydrate frame are given by

$$K_{hm} = K_{hKT}[(\phi_h/\phi)]^p \tag{16}$$

and

$$\mu_{hm} = \mu_{hKT}[(\phi_h/\phi)]^p, \tag{17}$$

where K_{hKT} and μ_{hKT} are the Kuster and Toksöz moduli when water is totally frozen, and the solid is replaced by air, i.e.

$$\frac{K_{hKT}}{K_h} = \frac{1 + [4\mu_h(K_a - K_h)/(3K_a + 4\mu_h)K_h](1 - \phi)}{1 - [3(K_a - K_h)/(3K_a + 4\mu_h)](1 - \phi)} \tag{18}$$

and

$$\frac{\mu_{hKT}}{\mu_h} = \frac{\phi\mu_h(9K_h + 8\mu_h)}{9K_h + 8\mu_h + (1 - \phi)(6K_h + 12\mu_h)} \tag{19}$$

(Kuster and Toksöz 1974), where K_a denotes the bulk modulus of air. (The bulk modulus of air used in this work is K_a = 0.15 MPa.)

In contrast, the P-wave velocity of the rock saturated with free gas, below the bottom-simulating reflector, is obtained with the classical Gassmann modulus (Carcione 2001, p. 225). The density and bulk modulus of free gas are obtained from van der Waals' equation as a function of pressure and temperature (e.g. Gei and Carcione 2003), and Wood's model is used to obtain the bulk modulus of the water/gas mixture (Mavko *et al.* 1998, p. 112). Alternatively, we can use Hill's average to evaluate the saturation for gas distributed in patches (Mavko *et al.* 1998, p. 115).

ESTIMATION OF GAS HYDRATE AND FREE GAS

The 3D depth distribution of seismic-wave velocity was obtained by reflection tomography. The method is based on Fermat's principle and represents the earth as a blocky medium, with reflecting curved or dipping interfaces. Adaptive and staggered grids enable the resolution of the velocity field to be enhanced without decreasing the stability of the inversion procedure. Vesnaver and Böhm (2000) have described the method. In order to obtain the velocity field, we chose 10 reflection events, four above the bottom-simulating reflector and six below the bottom-simulating reflector. Figure 1 shows the location and bathymetric map of the study area. Because the ocean-bottom seismometer (OBS) array is located on a relatively small central part of the area illuminated by the 3D survey, the OBS and single-channel data are jointly inverted in order to constrain the velocity field and interface geometries, respectively. Moreover, since the raypaths are mainly in the ocean (the water-column thickness is 1400 m), we perform a 'datuming' at 1200 m below sea-level (Rossi *et al.* 2004).

Figure 2 shows the two seismic profiles, represented by thick lines in Fig. 1. The bottom-simulating reflector is well defined, particularly in profile 1 where it cuts the dominant stratigraphy. Moreover, the lower frequency response due to gas-charged beds is identifiable below the bottom-simulating reflector in both seismic sections. Two vertical sections of the P-wave velocity cube are shown in Fig. 3. They correspond to the central parts of the seismic profiles shown in Fig. 2. The material properties of the individual constituents are given in Table 1. The average water velocity down to the sea-bottom has been estimated as 1462 m/s and the sea-bottom temperature is nearly −1°C (measured during the survey). The model requires calibration of the dry-rock bulk and rigidity modulus of the host sediment at full water saturation. The nearest calibration point is ODP well 986 (see location in Fig. 1) (Jansen *et al.* 1996). Four holes were drilled, with a maximum penetration of 964 mbsf. The sediments recovered are predominantly fine- to coarse-grained siliclastics with varying amounts of gravel. Unit II (98–562 mbsf), where the bottom-simulating reflector is located, is composed of silty clays with dropstone inclusions. The data indicate a temperature gradient of 100°C/km (G. Westbrook, pers. comm.), which is used to obtain the bulk modulus and density of free gas (assumed to be pure methane) from van der Waals' equation (Gei and Carcione 2003). Moreover, a sediment core 5.4 m long was collected from the sea-bottom. X-ray diffraction analysis on this core provided the following information: 48% clay content, 11% calcite content and 41% quartz content. The porosity value of 45% was obtained from Fig. 25 of Jansen *et al.*

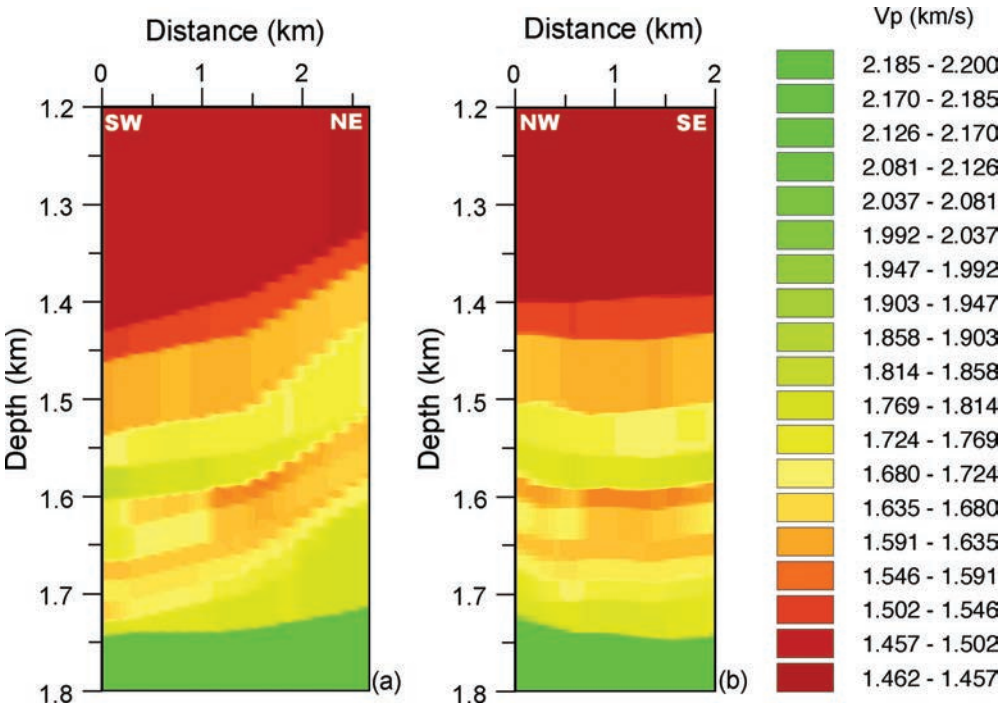

Figure 3 Tomographic P-wave velocity sections corresponding to the seismic lines shown in Fig. 2.

Table 1 Material properties

Grain	Bulk modulus, K_s	29.8 GPa
	Shear modulus, μ_s	18.0 GPa
	Density, ρ_s	2623 kg/m^3
Gas hydrate	Bulk modulus, K_h	7.7 GPa
	Shear modulus, μ_h	3.2 GPa
	Density, ρ_h	910 kg/m^3
Water	Bulk modulus, K_w	2.24 GPa
	Density, ρ_w	1030 kg/m^3
Free gas	Bulk modulus, K_g	21 MPa
	Density, ρ_g	130 kg/m^3

(1996). In order to compute the bulk modulus of the solid part, we assume 21 GPa for clay, 74.8 GPa for calcite and 36 GPa for quartz, and the densities are 2580, 2712 and 2650 kg/m^3, respectively. The respective shear moduli are assumed to be 6.9 GPa for clay, 30.6 GPa for calcite and 45 GPa for quartz. Wet-rock Poisson's ratios of 0.49 at the sea-bottom and 0.44 below the bottom-simulating reflector are used. These values were estimated by ray-tracing traveltime inversion (G. Westbrook, pers. comm.). The intermediate values are obtained by linear interpolation. The small difference in Poisson's ratio between the sea-bottom sediment and the sediment below the bottom-simulating reflector indicates that, in the present case, Poisson's ratio cannot discriminate between hydrate and free-gas bearing sediments (see e.g. Dvorkin *et al.* 2003, in which impedance–Poisson's-ratio cross-plots are used to identify gas hydrate and free gas). A possible explanation is that in our case the amount of gas hydrate is not sufficient to cement the sand grains and increase the S-wave velocity, so this is essentially constant through the bottom-simulating reflector. In addition, the P-wave velocity contrast at the bottom-simulating reflector is also small (nearly 200 m/s), which, together with the low value of the S-wave velocity (440 m/s), is not enough to cause a significant change in Poisson's ratio between the hydrate and free-gas bearing sediments. We must also consider the influence of possible errors which affect the calculation of the tomographic velocities, namely, the positioning of the OBS, the determination of the sound velocity of water, the relatively deep sea-bottom, traveltime-pick errors, and the relatively short offsets used to determine the S-wave velocity from the PS reflection event.

The values $K_0 = 2.8$ MPa, $K_\infty = 7$ GPa and $p^* = 13$ MPa are obtained from the sonic-log data collected at ODP well 986 at two different depths, i.e. near the sea-bottom and below the bottom-simulating reflector. Figure 4 compares the tomographic P-wave velocity (solid line), the reference velocity (dashed line, corresponding to full water saturation) and Hamilton's reference velocity (dotted line), at the intersection between the seismic profiles shown in Fig. 1.

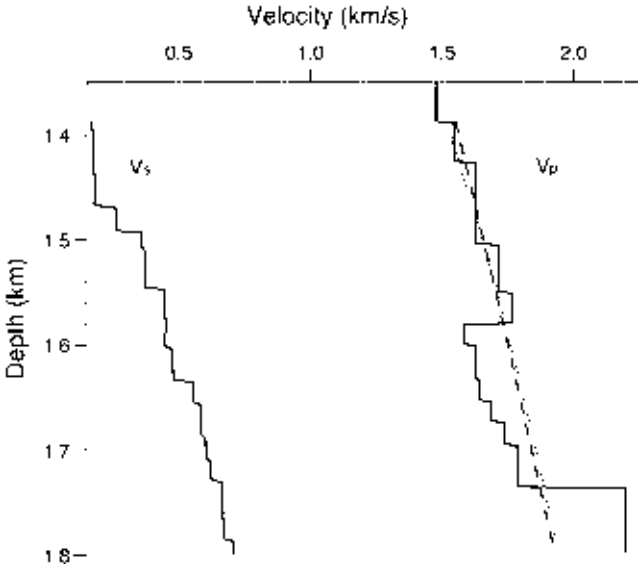

Figure 4 Tomographic velocity profiles (solid lines), reference velocity (dashed curve) and Hamilton velocity profiles (dotted curve) (Hamilton 1979) at the intersection between the seismic profiles shown in Fig. 1.

The bottom-simulating reflector is located approximately 1580 m below sea-level, where the tomographic P-wave velocity abruptly decreases. The reference velocity profile, considering fully water-saturated sediments, is assumed to be constant over the whole survey area. Discrepancies between the reference and the tomographic velocities are related to the presence of hydrate and free gas in the pores, above and below the bottom-simulating reflector, respectively.

The sections of gas-hydrate concentration (blue) and free-gas saturation (red) are shown in Fig. 5. We have obtained hydrate concentrations of up to 25%, with an average value of 7.2%. The higher and average values of free-gas saturation are 0.42% and 0.16%, respectively. The gas-hydrate content varies significantly across the section. The highest gas-hydrate concentration is obtained near the bottom-simulating reflector. Gas-hydrate concentrations cannot be confirmed by direct measurements because there are no well data of the survey area. However, comparable results have been obtained in the Storegga area, using a different rock-physics model (Bünz and Mienert 2004).

The gas-saturation values are highly dependent on the type of model used to obtain the velocity of the partially saturated

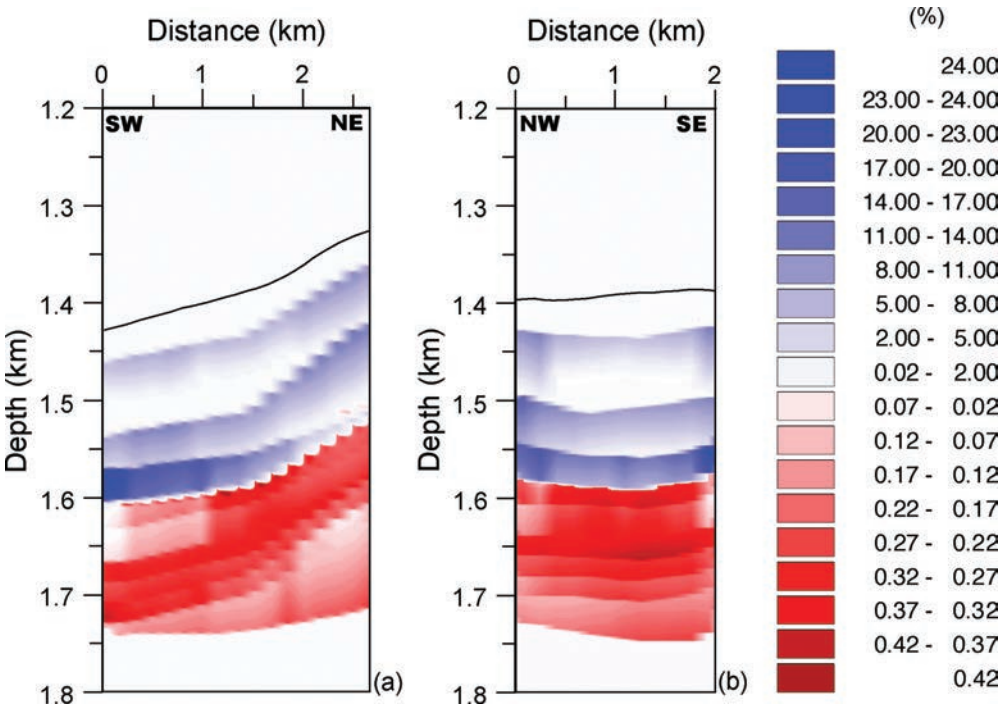

Figure 5 Sections of gas-hydrate concentration (blue) and free-gas saturation (red) corresponding to the velocity sections shown in Fig. 3. The solid line indicates the sea-bottom.

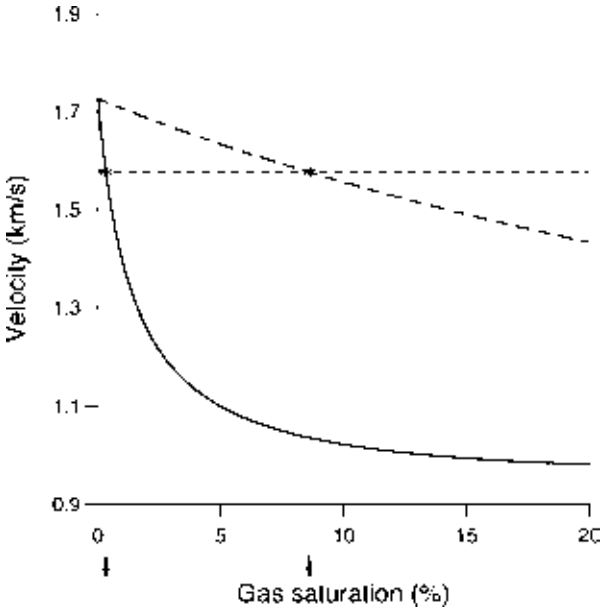

Figure 6 Wet-rock velocity of the partially saturated rock as a function of gas saturation. See text for description.

sediment. Figure 5 corresponds to Wood's model, i.e. a uniform mixture of gas and water within the pore space. If we use the patchy saturation model (Hill's model), the maximum free-gas saturation is nearly 9%. Patchy saturation implies an uneven distribution of fluids in the pore space and describes the response of a partially saturated medium. This is illustrated in Fig. 6, which shows the P-wave velocity of the partially saturated sediment as a function of gas saturation. The solid line corresponds to Wood's model and the dashed line to Hill's model. The horizontal dashed line is the tomographic velocity at 1.6 km depth (see Fig. 4), and the arrows indicate the saturation values obtained with each model. The estimation of gas saturation also depends on the pore pressure, since the density of the gas increases with depth. The difference in saturation between 1.6 km depth and 4 km depth, due to this density effect, can be up to one order of magnitude.

CONCLUSIONS

We have estimated the concentration of gas hydrate and saturation of free gas at the western Svalbard margin, using a three-phase poro-elastic model. We obtained hydrate concentrations of up to 25% and free-gas saturations of up to 0.42% (Wood's model) and 9% (Hill's model). The prediction relies on the tomographic P-wave velocities, and the calibration (evaluation of the dry-sediment bulk modulus) is based on the inverse Gassmann equation at full water saturation and *in situ* pressure conditions. The estimation of the gas

saturation is dependent on the kind of model used to describe the distribution of gas in the pore space, and is also sensitive to the pore pressure.

ACKNOWLEDGEMENTS

This work was supported by the European Union under the HYDRATECH project (contract number EVK3-CT-2000-00043). We thank all the participants in the acquisition and processing of the data used in this paper and, in particular, Graham Westbrook for his detailed review of the manuscript.

REFERENCES

Arbabi S. and Sahimi M. 1988. Elastic properties of three-dimensional percolation networks with stretching and bond-bending forces. *Physical Review B* **38**, 7173–7176.

Brown K.M. 1990. The nature and hydrogeologic significance of mud diapirs and diatremes for accretionary systems. *Journal of Geophysical Research* **95**(B6), 8969–8982.

Bünz S. and Mienert J. 2004. Acoustic imaging of gas hydrate and free gas at the Storegga Slide. *Journal of Geophysical Research* **109**(B04102), doi: 10.1029/2003JB002863.

Butt F.A., Elverhøi A., Solheim A. and Forsberg C.F. 2000. Deciphering Late Cenozoic development of the Western Svalbard Margin from ODP site 986 results. *Marine Geology* **169**, 373–390.

Carcione J.M. 2001. *Wave Fields in Real Media: Wave Propagation in Anisotropic, Anelastic and Porous Media*. Handbook of Geophysical Exploration, Vol. 31. Pergamon Press Inc.

Carcione J.M. and Gei D. 2004. Gas hydrate concentration estimated from P- and S-wave velocities at the Mallik 2L-38 research well, Mackenzie Delta, Canada. *Journal of Applied Geophysics* **56**, 73–78.

Carcione J.M. and Tinivella U. 2000. Bottom simulating reflectors: seismic velocities and AVO effects. *Geophysics* **65**, 54–67. *Errata*: **66**, 984 (2001).

Chand S., Minshull T.A., Gei D. and Carcione J.M. 2004. Elastic velocity models for gas-hydrate-bearing sediments: a comparison. *Geophysical Journal International* **159**, 573–590.

Dvorkin J., Nur A., Uden R. and Taner T. 2003. Rock physics of a gas hydrate reservoir. *The Leading Edge* **22**, 842–847.

Gei D. and Carcione J.M. 2003. Acoustic properties of sediments saturated with gas hydrate, free gas and water. *Geophysical Prospecting* **51**, 141–157.

Grevemeyer I. and Villinger H. 2001. Gas hydrate stability and the assessment of heat flow through continental margins. *Geophysical Journal International* **145**, 647–660.

Hamilton E.L. 1979. V_P/V_S and Poisson's ratios in marine sediments and rocks. *Journal of the Acoustical Society of America* **66**, 262–280.

Hashin Z. and Shtrikman S. 1963. A variational approach to the theory of the elastic behaviour of multiphase materials. *Journal of Mechanics and Physics of Solids* **11**, 127–140.

Jansen E., Raymo M.E., Blum P. and Shipboard Scientific Party, Ocean Drilling Program, Leg 162, Site 986 1996. *Proceedings of the Ocean Drilling Program*, Initial report, Vol. 162.

Kuster G.T. and Toksöz M.N. 1974. Velocity and attenuation of seismic waves in two-phase media: Part I. Theoretical formulations. *Geophysics* **39**, 587–606.

Kvenvolden K.A. 1993. Gas hydrates – geological perspective and global change. *Review of Geophysics* **31**, 173–187.

Leclaire Ph., Cohen-Ténoudji F. and Aguirre-Puente J. 1994. Extension of Biot's theory of wave propagation to frozen porous media. *Journal of the Acoustical Society of America* **96**, 3753–3768.

Leclaire P., Cohen-Ténoudji F. and Aguirre-Puente J. 1995. Observation of two longitudinal and two transverse waves in a frozen porous medium. *Journal of the Acoustical Society of America* **97**, 2052–2055.

Lodolo E., Camerlenghi A. and Brancolini G. 1993. A bottom simulating reflector on the South Shetland margin, Antarctic Peninsula. *Antarctic Science* **5**, 207–210.

Lundin E. and Doré A.G. 2002. Mid-Cenozoic postbreakup deformation in the passive margins bordering the Norwegian-Greenland Sea. *Marine and Petroleum Geology* **19**, 79–93.

Mavko G., Mukerji T. and Dvorkin J. 1998. *The Rock Physics Handbook: Tools for Seismic Analysis in Porous Media*. Cambridge University Press.

Mienert J. and Posewang J. 1999. Evidence of shallow- and deep-water gas hydrate destabilizations in North Atlantic polar continental margin sediments. *Geo-Marine Letters* **19**, 143–149.

Posewang J. and Mienert J. 1999. High-resolution seismic studies of gas hydrates west of Svalbard. *Geo-Marine Letters* **19**, 150–156.

Rossi G., Madrussani G., Böhm G. and Camerlenghi A. 2004. Tomographic inversion of OBS data offshore Svalbard Islands. 66th EAGE conference, Paris, France, Extended Abstracts, P218.

Rossi G., Madrussani G. and Camerlenghi A. 2003. Tomographic approach to the detection of gas hydrates offshore Western Svalbard. *Geophysical Research Abstracts* **5**, EGS 04225.

Stoll R.D., Ewing J. and Bryan G.M. 1971. Anomalous velocities in sediments containing gas hydrates. *Journal of Geophysical Research* **76**, 2090–2094.

Vanneste M., Mienert J., Guidard S. and HYDRATECH-INGGAS partners 2002. 'Arctic' gas hydrate offshore Western Svalbard, Norway. *Proceedings of the 4th International Conference on Gas Hydrates*, Yokohama, Japan, pp. 222–227.

Vesnaver A. and Böhm G. 2000. Staggered or adapted grids for seismic tomography? *The Leading Edge* **19**, 944–950.